Opportunities in Science using a Soft X-ray FEL

W. Eberhardt
IFF, Forschungszentrum Jülich
D-52425 Jülich, Germany

Extrapolating from our present research program, I will illustrate some scientific areas, where a FEL source will create some unique opportunities for novel experiments. The examples given make use of either the coherence, or the peak power and time structure of the FEL source. As specific examples element selective studies of the magnetization dynamics in ultrathin films and multilayers of relevance for magnetoelectronics are discussed.

Over the past decades the power and brilliance of synchrotron radiation sources has increased by many orders of magnitude as illustrated by Fig. 1. Even the average photon flux at the sample at the state of the art synchrotron sources exceeds by far the flux available from the most powerful laboratory sources. Now, at the eve of the new millenium, another dramatic increase in the flux and brightness of X-ray beams is promised by the X-FEL. The predicted beam characteristics, with respect to pulse length, peak power or respectively the number of photons per pulse, of a soft or hard X-ray FEL match for the first time properties of state of the art high power, short pulse length laboratory lasers. The FEL however offers the unique feature that the photon energy is several orders of magnitude larger than for conventional lasers. The properties of a state of the art synchrotron source, a laboratory laser system, and the FEL are summarized in Table 1. From this comparison it is immediately apparent, that the various experimental techniques, such as non-linear and pump-probe spectroscopies now can be extended to the VUV, as well as the soft and hard X-ray photon energy range. As reflected by the award of the Nobel prize in chemistry this year these sec pump-probe studies have already produced very exciting results using visible and near UV photons. Furthermore, the coherence of these FEL sources will be orders of magnitude larger than at conventional state of the art synchrotron sources.

Accordingly, in the following I will describe some experiments that make use of either the coherent properties or the peak power and time structure of the FEL in order to highlight the opportunities for novel experiments at an X-FEL source. The examples given are based upon extrapolations of our current research program and therefore just reflect one particular field of interest, the studies of magnetic thin film systems used in magnetoelectronic applications. Magnetoelectronics has developed over the past years into a rapidly expanding field of technology oriented science. Based upon the special magnetic properties of thin films and multilayer systems novel types of devices have been created, whereby not only the charge but also the spin of the electrons is used for information processing and storage. Foremost among these are magnetic sensors based upon the GMR-effect (Giant-Magneto-Resistance)[1,2] and the development of MRAM (Magnetic Random Access Memory) non volatile memory devices [3]

A. Scattering with coherent photons (SPECKLE)

The first area of applications of the special properties of the FEL source concerns scattering of coherent photons from samples having a unique surface or interface morphology. It is well known from laser scattering of visible photons, that using a coherent light source, the light scattered from a sample exhibits pronounced interference effects. Due to the coherence the phase information, which is usually not obtained in a scattering experiment is recorded in the observed interference (speckle-) pattern similar to a hologram. In principle, from the reconstruction of this interference pattern, the unique and individual sample morphology should be obtainable. The size range of the preferentially contributing structures and the spatial resolution is determined by the momentum transfer in the photon scattering event. The size range basically scales with the wavelength used in the scattering experiment. Accordingly shorter wavelengths will immediately translate into improved resolution for this type of measurement.

Laboratory laser sources providing coherent radiation in the visible and near UV range have been used extensively for speckle spectroscopy. At higher energies (shorter wavelengths) only synchrotron radiation is available as a moderately powerful coherent source, whereby in most scattering experiments so far the coherent properties of the synchrotron radiation have not yet played any role. Exploiting the coherence of the synchrotron radiation adds another dimension to the investigation of the structure and dynamics of matter. At present day 3rd generation undulator sources this property is just starting to be explored. This coherent flux will further improve by orders of magnitude once radiation from free electron lasers in the X-ray range becomes available.

Recently some first coherent scattering experiments were carried out using hard X-rays in transmission through a sample [4] or reflection from a surface [5]. We have demonstrated the first use of speckle spectroscopy in the soft X-ray energy range [6] which we believe offers some unique opportunities for the investigations of dynamical processes at surfaces or shallow buried interfaces. This is emphasized by the following brief considerations.

The momentum transfer $\mathbf{q} = (\mathbf{q}_x,\mathbf{q}_y,\mathbf{q}_z)$ in the photon scattering event is given by Eq. 1, where θ_i and θ_f are the angles of incidence and detection of the radiation respectively, measured relative to the surface. The plane of incidence is given by the xz-plane and ϕ is the angle of deflection of the scattered beam measured relative to the plane of incidence

$$\mathbf{q}_z = 2\pi/\lambda\ (\sin\theta_i + \sin\theta_f)$$

$$\mathbf{q}_x = 2\pi/\lambda\ (\cos\theta_i - \cos\theta_f)\cos\phi \text{ and } \mathbf{q}_y = 2\pi/\lambda\ (\cos\theta_i - \cos\theta_f)\sin\phi$$

Compared to the use of visible laser radiation, soft X-rays have a larger momentum, typically by a factor of 10^2 to 10^3, which can be transferred to the sample, thus probing correlations at a correspondingly smaller length scale. Obviously along the same line of arguments, hard X-rays can supply even larger momenta, but, on the other hand, are limited in the application of speckle for different reasons. Hard X-rays can be used in transmission, whereby the whole sample is probed. In surface studies, or for investigations of buried interfaces, very grazing

angles of incidence have to be used because of the low reflectivity for hard X-rays, which severely limits the q-range of the experiments [7].

Before describing any of these experiments in more detail we first have to introduce the concept of coherence as it applies at a synchrotron radiation source. In general, synchrotron radiation from undulators contains a coherent superposition of photons emitted along the electron trajectory in the storage ring. This is responsible for the "spikes" in the undulator spectrum compared to the smooth, slowly varying emission characteristics from a normal bending magnet source. Nevertheless this natural spectrum of the undulator emission quite often is not sufficient for performing experiments with coherent photons. In order to establish the uniformity of the wavefront observed along the beam (or in the time domain) the photon wavelength needs to be additionally restricted by a monochromator. This is also referred to as "longitudinal coherence". Given a certain wavelength resolution $\Delta\lambda$, the longitudinal coherence length L_L is simply defined as

$$L_L = \lambda^2/\pi\Delta\lambda$$

At an FEL, the natural linewidth might produce a sufficient amount of coherent flux, especially when seeded operation is available.

Additionally, the phase of the electromagnetic field across the photon beam (and thus the sample) has to be well defined. This is also called "transverse coherence". In conjunction with a well defined source this can be achieved by placing a small aperture with diameter D at the distance S from the source into the beam, selecting only the central cone of the undulator emission. Alternately two apertures placed along the beam may be used. The lateral (transverse) coherence length L_T is given by

$$L_T = \lambda S/\pi D$$

Incidentally by these measures any light source can be made coherent. The main distinction however is the photon flux that survives this stringent selection and reaches the sample.

At the X1B undulator at the NSLS Brookhaven we performed some tests of these principles. We placed two pinholes with diameters of 100μm and 20μm, 660 mm apart, into the beam behind the exit slit of the monochromator. The wavelength was somewhat arbitrarily selected to be 5.77 nm, the main reason for this selection being to avoid the reduction in flux by carbon contamination of the beamline optical elements. In order to verify that the transmitted photon flux is largely coherent, according to the definitions given above, we recorded the diffraction pattern observed about 0.4 m downstream of the last pinhole with a two-dimensional soft X-ray detector. This detector is our standard soft X-ray channelplate detector with a resistive anode mounted on a two-dimensional linear slide arrangement. The spatial resolution of this detector is about 20 μm horizontally and 80 μm vertically. The diffraction pattern is shown in a logarithmic false color representation in Fig. 2. A series of rings is clearly visible in this pattern, corresponding to a Fraunhofer diffraction pattern from a reasonably circular aperture. Thus we unambiguously are able to demonstrate that the predominant photon flux, selected as described above, is indeed coherent.

This last observation can even be described in a quantitative fashion. Modeling the diffraction pattern of this aperture in the far field, the actual coherence length can be determined as illustrated in Fig. 3. Here the diffraction pattern is modeled using different lateral coherence lengths. From this comparison a coherence length of 20 μm seems to agree best with the experiment. Obviously larger coherence lengths result in sharper diffraction fringes, and smaller values give a more washed out pattern.

Fig.4 shows a coherent scattering pattern taken from a porous Si sample, prepared as described previously [8]. The sample was placed just a few mm downstream of the last pinhole and could be rotated about an axis in the surface and perpendicular to the photon beam. Using this setup the angle of incidence on the sample could be varied and the detector could be scanned to follow the direct scattered beam. For the "speckle" pattern from the porous Si sample shown in Fig. 4, the beam was incident under a glancing angle of 9^{o} onto the sample and the detector was placed about 40 cm downstream of the sample. The

asymmetry of the observed speckle pattern can be readily explained by the momentum transfer equations given above. In general, the momentum space is expanded along the plane of incidence, giving rise to the characteristic oval shape of the speckle pattern.

This speckle pattern is a unique representation of the sample. Similar to a hologram all the information is contained in this pattern. However, since it was recorded without a reference wave, the reconstruction is not straightforward. There are various efforts being undertaken presently to develop an algorithm for such a reconstruction [9]. Even without a complete reconstruction, there is still information to be extracted from this speckle pattern. In a slightly simplified view, the scattering in the plane of incidence and perpendicular to it can be treated separately. In the scattering plane the variations of the speckle pattern are largely determined by the vertical correlation function of the sample, whereas normal to the scattering plane the in-plane correlations play a major role. Even more simplified, the intensity of the central peak measured relative to the intensity variations in off specular directions is a direct measure of the smoothness of the sample. If the surface is rough on the scale the surface is probed, the specular intensity is low compared to the off specular intensity. A perfect smooth and flat surface on the other hand, will give rise to a large intensity specular reflected beam. Quantitatively, for example modeling the intensity trace shown at the bottom of Fig. 4 and using the appropriate parameters of this particular scattering experiment one derives at a (vertical) surface roughness value of $\sigma = 6.7$ nm.

As already mentioned above, various groups are presently just beginning to explore the use of speckle spectroscopy. Even if a unique reconstruction of the sample will not be achieved in the future, speckle will still give very valuable information as far as dynamic processes are concerned. With present day undulator sources a speckle pattern can be recorded taking anywhere from msec's to a few sec's total data acquisition time. In approaching a phase transition of the sample, many speckle patterns may be recorded consecutively, recording the change of the correlation lengths as the phase transition is encountered.

In the context of magnetoelectronics the interface of ferromagnetic layers with antiferromagnets, such as Co/NiO, poses many interesting unresolved questions. These exchange bias configurations play an important role in so called spin-valve systems, by pinning the orientation of the magnetic alignment of the ferromagnetic layer at the interface with the antiferromagnet. The exact mechanism of this pinning however is not yet understood microscopically. In sensors the exchange bias configuration serves to keep the magnetic orientation of one magnetic layer at a fixed spatial direction, while the second (soft) magnetic layer in the sensor is rotated under the influence of an external magnetic field. Obviously this only works in fields smaller than the bias field of the spin valve system. Controlling this effect is therefore an important goal in the actual device fabrication.

Using coherent light scattering as a probe, the domain configurations and dynamics of e.g. Co/NiO exchange bias layers can be studied in a unique and correlated way. MLD (Magnetic Linear Dichroism) offers a contrast mechanism for the scattering of domains of an antiferromagnet [10], while CMXD (Circular Magnetic X-ray Dichroism) provides the contrast for the magnetic film. Switching the polarization of the X-ray beam, for example, the dynamics of the domain configurations in both films can be studied simultaneously as the system is heated through the Neel temperature of the antiferromagnet.

Another interesting application of speckle spectroscopy is the study of phase transitions in polymers or liquid crystals, where also the first experiments have just been completed [11]. By the time a (soft-) X-ray FEL is available I would hope that many more groups are fascinated with the possibilities offered by this novel technique. Again for complex samples, the tunability of the synchrotron radiation source might come in very handy by offering the possibility to study dynamical processes combined with element specificity.

B. Time resolved pump-probe experiments

The second class of experiments that will benefit greatly from a FEL source are time resolved pump-probe experiments. Again, also in this class of experiments one can dream about many fascinating possibilities. As an example I will just describe one of our own time resolved investigations [12] and try to extrapolate from this viewpoint. The example I have chosen deals with the basic atomic scale processes and the time limitations of the magneto optical recording process.

Magneto-optical recorders, also called Mini-disc recorders, have recently attracted a lot of commercial attention, especially among the younger consumer crowd. In these digital information is stored in a magnetic medium and retrieved by a laser scanning over the medium. The MOKE (Magneto Optical Kerr Effect) signal reveals the bit orientation of the magnetic medium. The same laser beam, even though with increased intensity is used for inscribing new information. Using a short laser pulse the ferromagnetic recording medium is locally heated up to the Curie Temperature T_c, where only small magnetic fields are required for magnetizing the recording medium while cooling down. The orientation of a weak external magnetic field can thus be inscribed locally into a newly created domain in the recording medium. Obviously the timescale of the demagnetization determines the fundamental speed limit for this information storage process.

Prior to the studies presented here very little and even partially contradicting results have been presented about the details of this demagnetization process Vaterlaus et al. determined the magnetization relaxation time in Gd to 100±80ps [13]. Additionally, they could estimate the relaxation times in Fe, like Ni an itinerant ferromagnet, to about 30 ps - 20 ns, which is also two orders of magnitude larger than the electron relaxation times. In a more recent experiment by Beaurepaire et al., however, a fast demagnetization of a thin Ni film upon laser heating on a timescale of about 1ps was reported [14]. This result was later verified by Hohlfeld et al. [15].

Our experimental approach to these questions was via a time resolved, spin polarized photoemission experiments with fsec time resolution, using a two photon photoemission setup, covering relaxation times from below 1ps up to 1ns. The experimental setup is schematically shown in Fig. 5. As a primary excitation source we used a Ti:Al_2O_3 laser system with a pulsed output of 4μJ/pulse, a photon energy of 1.5eV, and a pulse width of 170fs. In a first step the photon energy is doubled to 3eV and then the beam is split. One of the beams is used as the "pump" beam, to heat the sample. The optical path length of the second beam can be varied with respect to the heating beam by an optical delay line. The frequency of the "probe" pulse is doubled again to a photon energy of 6eV, so that single photon photoemission is possible. Both beams are than focused to the same point of the sample, with a diameter of 200 μm. Photoelectrons excited by the 6eV probe pulse are spin analyzed by a retarding Mott detector.

Spin polarized photoemission has been extensively used in investigating magnetic materials. In the adiabatic limit the relative change of the measured polarization of the photoelectrons upon temperature reflects the change of the sample magnetization. In a time resolved experiment using short laser heating pulses however, special care has to be used in relating spectroscopic results to equilibrium properties like the magnetization, especially for short delay times, when the system has not yet reached equilibrium.

Thin Ni films on Ag(100) were grown at room temperature by electron beam evaporation from a high purity Ni rod. The Ag substrate is chosen because of its large thermal conductivity and Ni because of its high spin polarization of the photoemitted electrons, which is above 30% at the probe energy of 6eV. As for all magnetic thin film systems, the Curie temperature of the Ni overlayer can be varied by growing films of different thickness.

Fig. 6 shows the normalized spin polarization of the photoemitted electrons for a film thickness of 6Å as function of the delay time between heating pulse and probe pulse. This film has a Curie temperature of approximately 360K. A background asymmetry, caused by instrumental asymmetries of the spin detector, as well as by electrons which are photoemitted in a two-photon process from the heating pulse, is subtracted. At short delay times the polarization exhibits a very steep drop, followed by a slower decrease for longer delay times. The width of the fast, step-like, decrease at time zero reflects the laser pulse width. The change in slope at 500ps is taken as indication that the Curie temperature has been reached.

Keeping in mind, that the electron - electron relaxation as well as the electron - lattice relaxation occur on sub psec timescales, the slow decrease observed in the curve shown in Fig. 6 has to be associated with a spin-lattice relaxation process. The relaxation time of several 100 psecs is in good agreement with the magnon frequencies of Ni. Furthermore this time constant also falls into the range estimated by Vaterlaus et al. [13].

Additionally, however a very fast demagnetization process must occur as well, in order to explain the very fast decrease of the spin polarization near time zero. To emphasize this point, in Fig. 7 the spin polarization is shown for a 12Å thick Ni film on an expanded timescale. Two additional features become visible. First, the sharp drop at time zero is followed by only a partial recovery in the measured spin polarization after about 4 psec. Subsequently the measured spin polarization remains nearly constant with possibly a broader, more shallow dip at about 20ps delay. Finally, the slow and steady decrease sets in which is more clearly observed on the longer timescales emphasized in Fig. 6.

In order to explain these data we have to realize that the measured spin polarization in our experiment is determined by the occupation of the electronic states integrated over an energy window starting at about 1 eV binding energy, measured relative to E_F. Ni as a strong

ferromagnet has no unoccupied majority d states. By absorption of the "pump" photons the high density of minority d states just above the Fermi edge is filled either by direct optical excitation or by Auger decay of deeper valence holes. Even though this clearly has an effect on the spin polarization as observed our experiment, this nevertheless cannot be interpreted as a change in the average total spin moment or the magnetization of the system, since to first order in all these optical excitation and Auger decay processes the spin of the electrons and holes is conserved. Consequently the drop of the spin polarization around 1ps can be assigned to mainly electronic excitations by the "pump" pulse.

The temporal width of the dip is accordingly determined by the thermalization time of the electrons and the holes. This is consistent with the observed slight recovery of the spin polarization on a timescale of a few p-sec. The important information in the curves shown in Figs. 6 and 7 however is that this recovery of the initial drop of the spin polarization is largely incomplete. This demonstrates the existence of a very fast process changing the actual average spin polarization beyond the change of the electronic occupation. Furthermore, this process stops at about the same time the electrons have thermalized. Otherwise the polarization would have to drop further and more steeply in the time range of a few tenths of psecs.

The mechanism of this fast spin relaxation process is presently understood as an electron electron spin-flip scattering process. Thereby spin is exchanged for orbital momentum thus conserving the total angular momentum while simultaneously lowering the magnetization. Spin-orbit coupling is essential for this exchange of angular momentum. This process also provides a mechanism, whereby the energy flow to the spin system stops after the first few psecs. The existence of the Stoner gap, which corresponds to the minimal energy for a single particle spin flip process, creates an energy barrier for the energy flow from hot electrons to the spin system. The Stoner gap of Ni is about 65 meV and this energy is equivalent to a temperature of 750K. As soon as the temperature of the thermalized electron - lattice system

is lower, single spin flip excitations become improbable. At longer times only the pathway vía electron-phonon and phonon-magnon scattering is open to transfer electronic and vibronic energy into the spin system.

Summarizing these fsec pump-probe studies, we observe three excitation mechanisms on a fsec to psec timescale on ferromagnetic thin Ni films, reducing the spin polarization of photoemitted electrons. Initially, a redistribution of the occupation of the electronic states by the optical absorption of the "pump" photons causes a narrow minimum in the spin polarization immediately after time zero. Additionally, demagnetization processes on two different timescales are observed. One is a very fast electron-electron scattering process on a sub psec timescale, whereby energy is transferred from the not yet thermalized or the thermalized, but hot electrons to the spin system. The second, slow process is readily attributed to the spin - lattice interaction on a timescale of a few hundred psec‘s. The observed total decrease of the magnetization is dependent on the Curie temperature of the film and the total laser power absorbed in the "pump" process.

The experiment described here was only one example, where processes on the fsec timescale have recently attracted a lot of attention. One other major area is the study of chemical processes on this timescale. This is the area where the 1999 Nobel prize in chemistry was awarded. There are obviously many more scientific opportunities, such as the observation of structural changes in biological systems upon absorption of light or following another stimulus. These kind of structural studies require fsec time resolution and X-rays as they will be provided by an X-ray FEL. First experiments of this kind are under way at various 3rd generation synchrotron radiation sources around the world, but they will obviously greatly benefit from the increased peak power of an X-ray FEL.

In closing, I want to thank all my collaborators who have carried out the experiments I used to illustrate the opportunities for the use of high intensity coherent and/or fsec (soft) X-ray

pulses. For the speckle experiments these are S. Eisebitt, A. Karl, R. Scherer, M. Adamcyk, M. Pistonesi, and T. Tiedje whereas the fsec magnetic studies were carried out by A. Scholl, L. Baumgarten, and R. Jacquemin.

Figure Captions

Fig. 1 Increase of the brightness of X-ray sources as various generations of synchrotron radiation sources are being developed. The abbreviations denote various typical sources.

Fig. 2 Diffraction pattern of a circular aperture taken with soft (5.7 nm) X-rays. The intensity is shown in a false color representation. The scattering plane is horizontal and a trace of the intensity along the scattering plane is shown on a logarithmic scale at the bottom

Fig. 3 Intensity trace taken through the center of the diffraction pattern similar to the one shown in Fig. 2 compared to a calculated trace assuming a lateral coherence length of 20 μm.

Fig. 4 Speckle pattern taken from a porous Si sample with 5.7 nm soft X-rays incident under a glancing angle of 9^{o}. A linear intensity trace along the (horizontal) scattering plane is shown at the bottom.

Fig. 5 Schematic of the two-photon fsec time resolved photoemission setup probing the spin-polarization of magnetic samples. Meanwhile our time resolution has been improved by at least a factor of 3.

Fig. 6 Time resolved photoemission spin polarization measured from a 6Å Ni film following pulsed laser excitation. The curves are normalized according to the procedure described in the original publication [12]

Fig. 7 Same as Fig. 6 but for a 12Å Ni film and plotted on an expanded time scale

Table 1

Properties of Laser and Synchrotron Light Sources

	Synchrotron Radiation	Laboratory Laser Source	(Soft-) X-ray FEL TESLA-TTF
Photon Energy	1 eV to >10 keV	1 eV up to 6 eV	10 - 500 eV
Photons/pulse	10^7 (monochromatic)	10^{15}	$4x10^{13}$ monochromatic
Number of pulses/sec	10^7	10 - 10^3	7200 micropulses with 10 Hz repeat
Pulse Length (psec)	50	100 fsec	250 fsec
Energy/Pulse	0.2 nJ	1 - 10 mJ at 10 - 10^3 Hz	1.25 mJ (200 eV)
Average Power	2 mW	1 W	90 W
Peak Power	3.2 W	100 GW	5 GW

References

1. M. N. Baibich, J. M. Broto, A. Fert, F. Nguyen van Dau, F. Petroff, P. Etienne, G. Creuzet, A. Friedrich and J. Chazelas, Phys. Rev. Lett. **61**, 2472 (1988)

2. P. Grünberg, R. Schreiber, Y. Pang, M.B. Brodsky, and H. Sowers, Phys. Rev. Lett. **57**, 2442 (1986) and B. Binasch, P. Grünberg, F. Saurenbach, W. Zinn, Phys.Rev.**B 39**, 4828 (1989)

3 G.A. Prinz, K. Hathaway, Physics Today, (April 1995): Special Issue on Magnetoelectronics

4 S. Bauer, G.B. Stephenson, M. Sutton, R. Brüning, E. Dufresne, S.G.J. Mochrie, G. Grübel, J. Als-Nielsen, D. Abernathy, Phys. Rev. Lett **74**, 2010 (1995)

5 M. Sutton, S.G.J. Mochrie, T. Greytag, S.E. Nagler, L.E. Berman, G.A. Heald, G.B. Stephenson,Nature **352**, 608 (1991)

6 S. Eisebitt, A. Karl, R. Scherer, W. Eberhardt, M. Adamcyk, T. Tiedje, M. Pistonesi, Synchr. Rad. News **11**, (No. 5) p.15 (1998)

7 J.L. Libbert, R. Pindak, S.P. Dierker, I.K. Robinson, Phys. Rev. **B56**, 6454 (1997)

8 S. Eisebitt, S.N. Patitsas, T. Tiedje, T. van Buuren, J. Lüning, J.E. Rubensson, W. Eberhardt, Europhys. Lett. **37**, 133 (1997)

9 I,K Robinson, J.L. Libbert, I.A. Vartanyants, J.A. Pitney, D.M. Smilgies, D.L. Abernathy, G. Grübel, Phys. Rev. **B60**, 9965 (1999)

10. J. Stöhr, A. Scholl, T.J. Regan, S. Anders, J. Lüning , M.R. Scheinfein, H.A. Padmore, R.L. White, Phys. Rev. Lett **83**, 1862 (1999)

11. A.C. Price, L.B. Sorensen, S.D. Kevan, J. Toner, A. Poniewierski, R. Holyst, Phys. Rev. Lett. **82**, 755 (1999)

12 A. Scholl, L. Baumgarten, R. Jacquemin, W. Eberhardt, Phys. Rev. Lett **79**, 5146 (1997)

13 A. Vaterlaus, T. Beutler, D. Guarisco, M. Lutz, F. Meier, Phys. Rev. **B46**, 5280 (1992)

14 E. Beaurepaire, J.C. Merle, A. Daunois, j.Y. Bigot, Phys. Rev. Lett. **76**, 4250 (1996)

15 J. Hohlfeld, E. Matthias, R. Knorren, K.H. Bennemann, Phys. Rev. Lett. **79**, 5149 (1997)

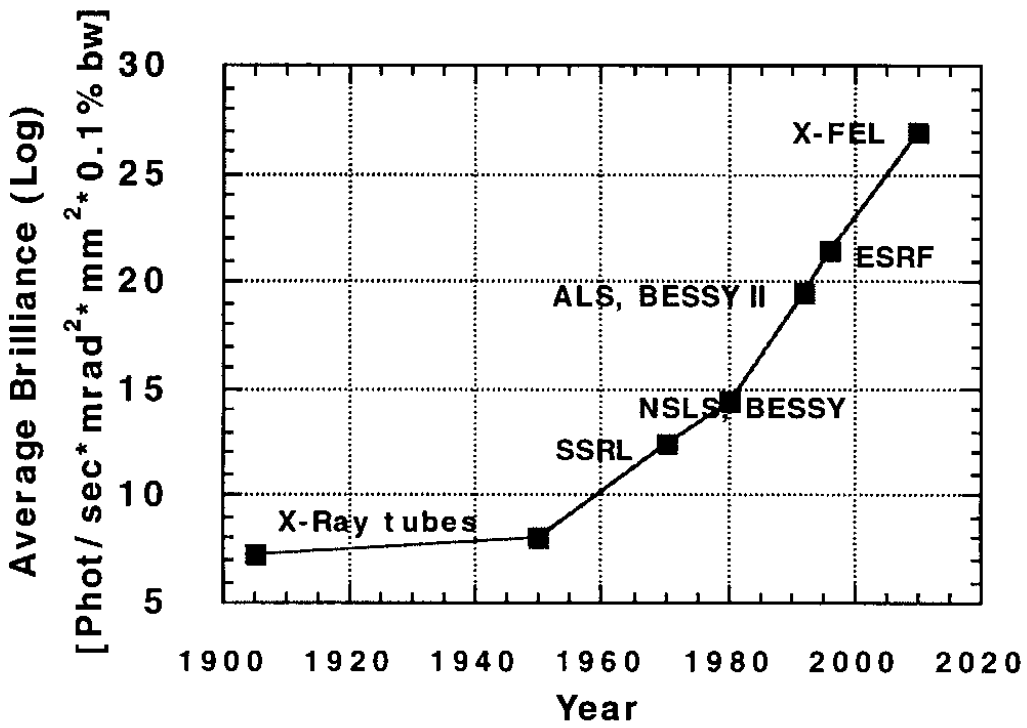
Average Brilliance (Log)
[Phot/ sec* mrad^2* mm^2* 0.1 % bw]
30
25
20
15
10
5
1900
1920
1940
1960
1980
2000
2020
Year
X-FEL
ESRF
ALS, BESSY II
NSLS, BESSY
SSRL
X-Ray tubes

Figure 1

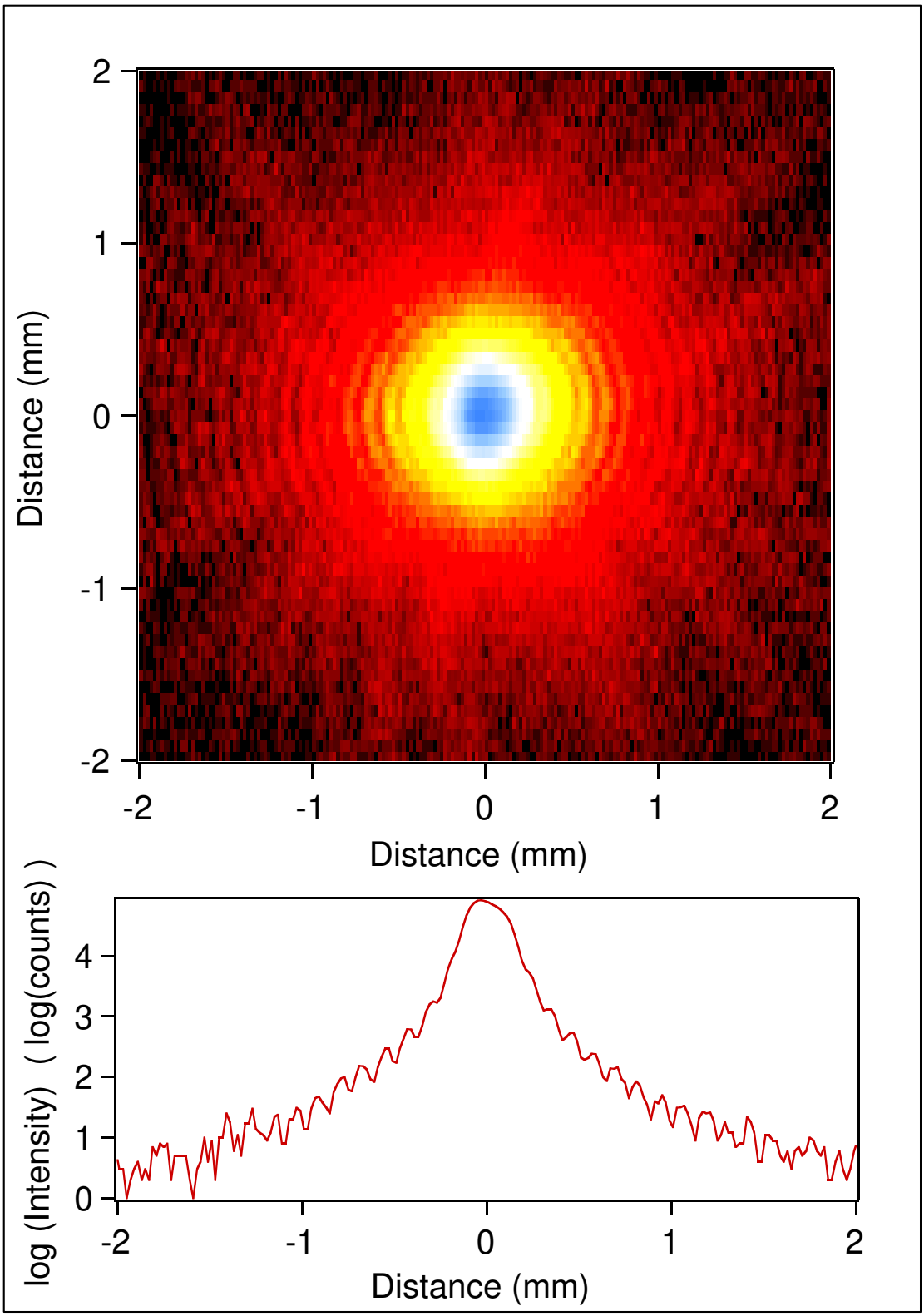
2
1
0
-1
-2
Distance (mm)
-2
-1
0
1
2
Distance (mm)
log (Intensity) (log(counts))
4
3
2
1
0
-2
-1
0
1
2
Distance (mm)

Figure 2

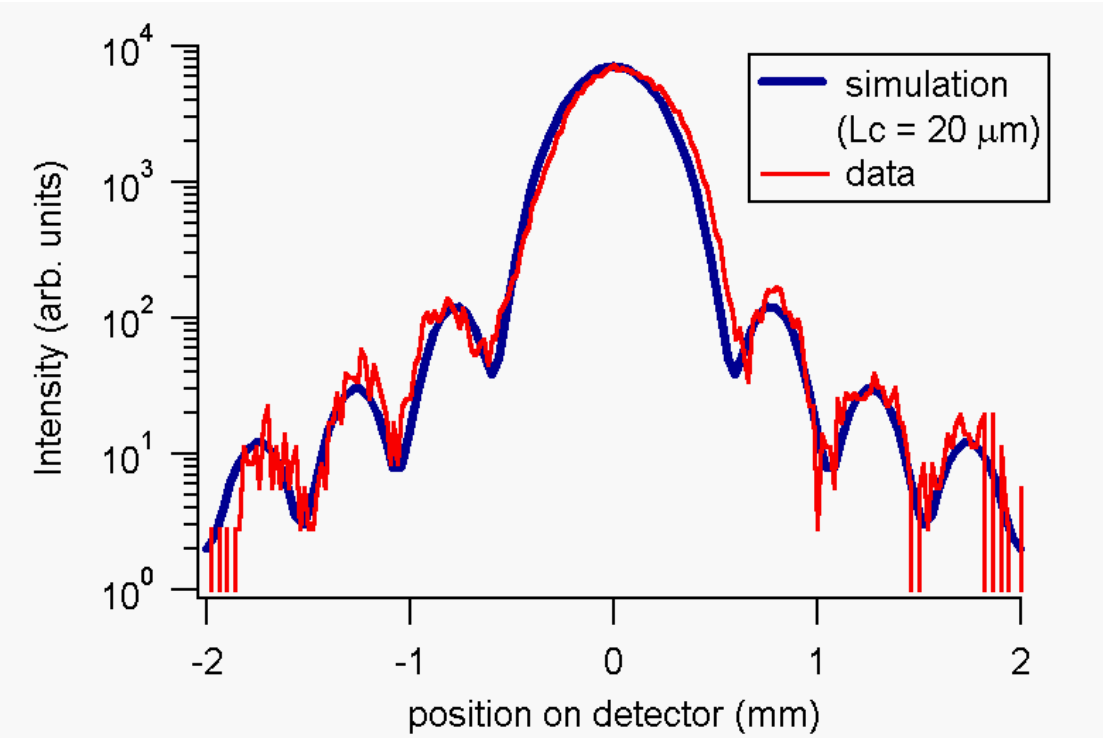
simulation
(Lc = 20 μm)
data
Intensity (arb. units)
10^4
10^3
10^2
10^1
10^0
-2
-1
0
1
2
position on detector (mm)

Figure 3

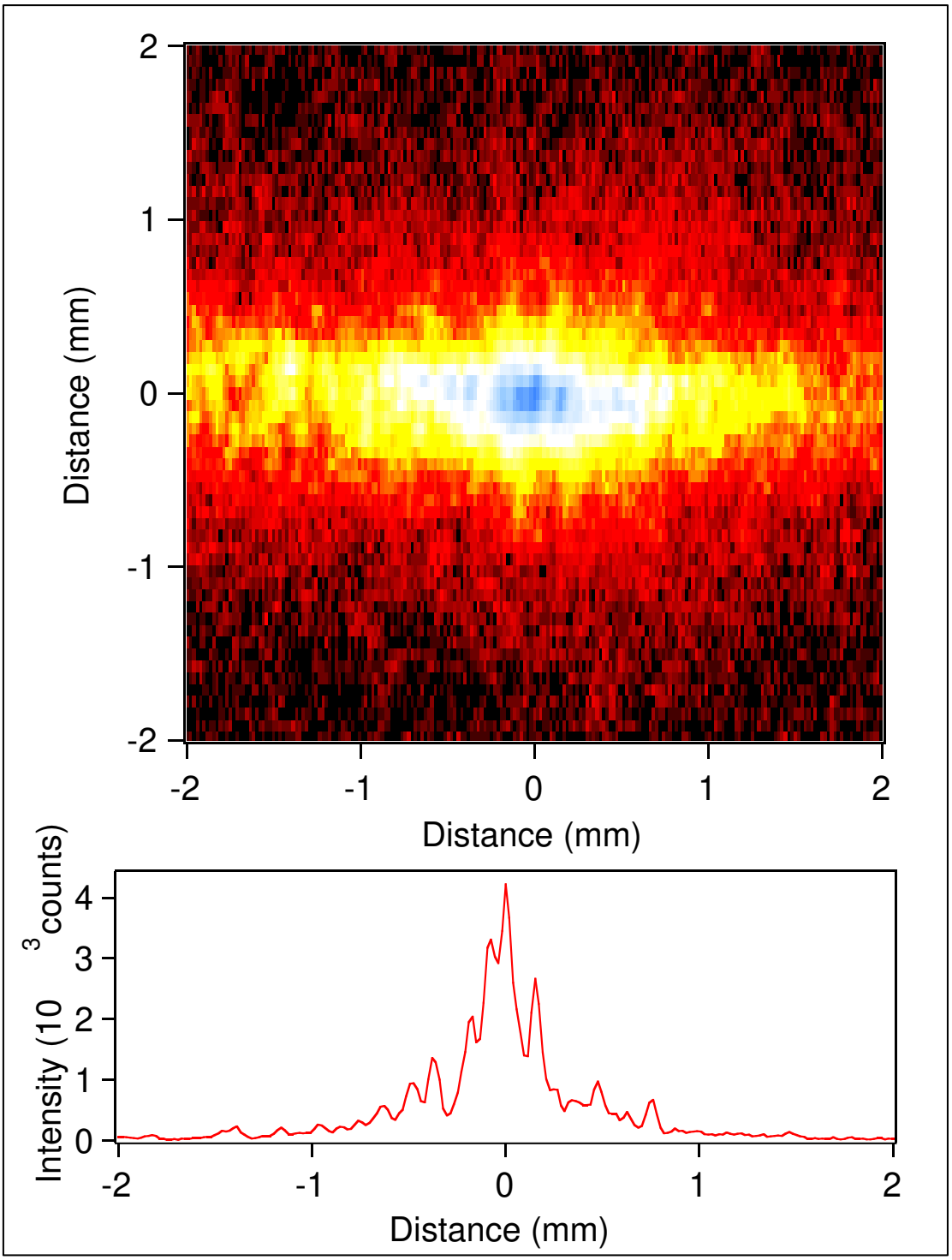
2
1
0
-1
-2
Distance (mm)
-2
-1
0
1
2
Distance (mm)
Intensity (10 3 counts)
4
3
2
1
0
-2
-1
0
1
2
Distance (mm)

Figure 4

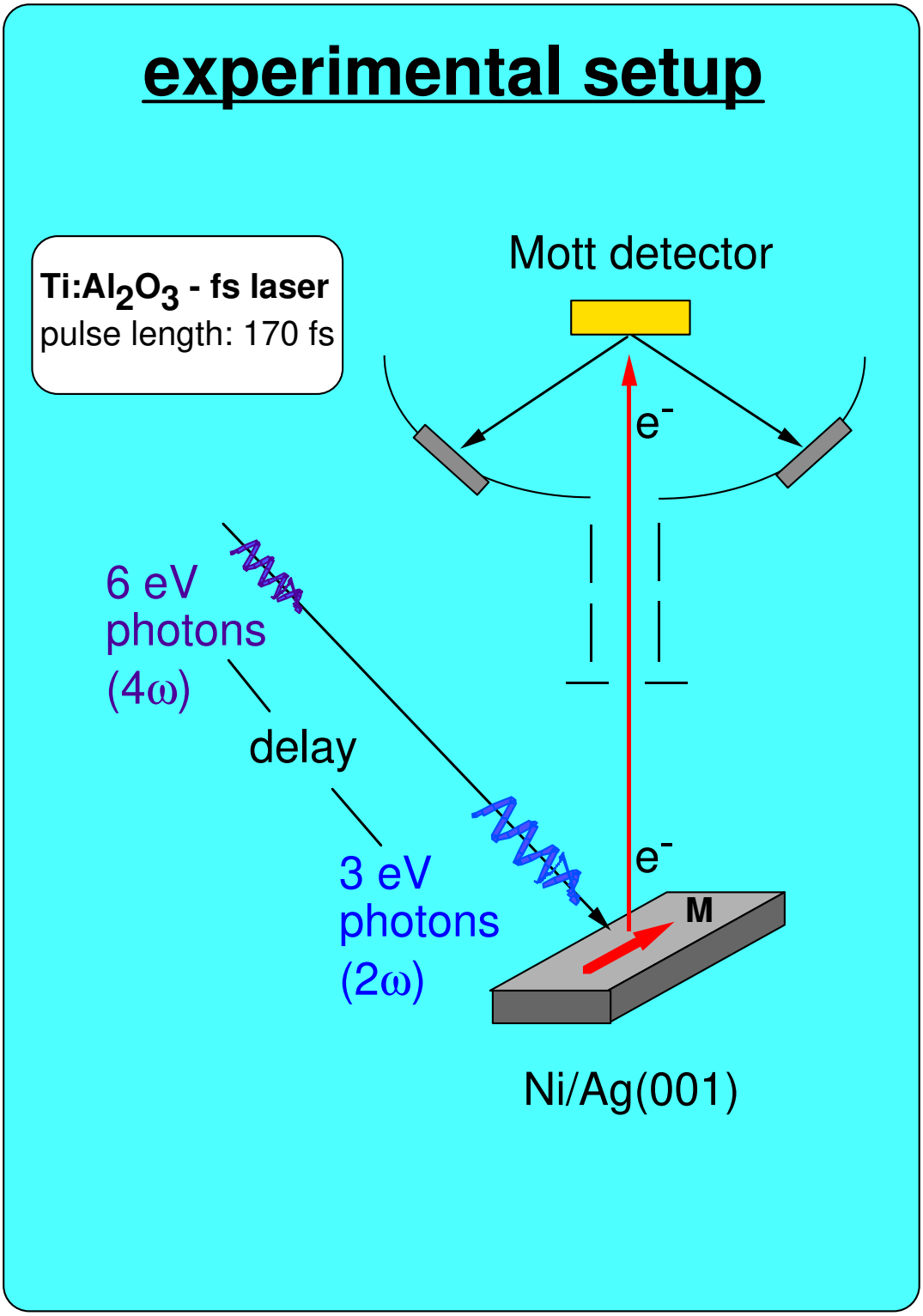
experimental setup
Ti:Al2O3 - fs laser
pulse length: 170 fs
Mott detector
e-
6 eV
photons
(4ω)
delay
3 eV
photons
(2ω)
e-
M
Ni/Ag(001)

Figure 5

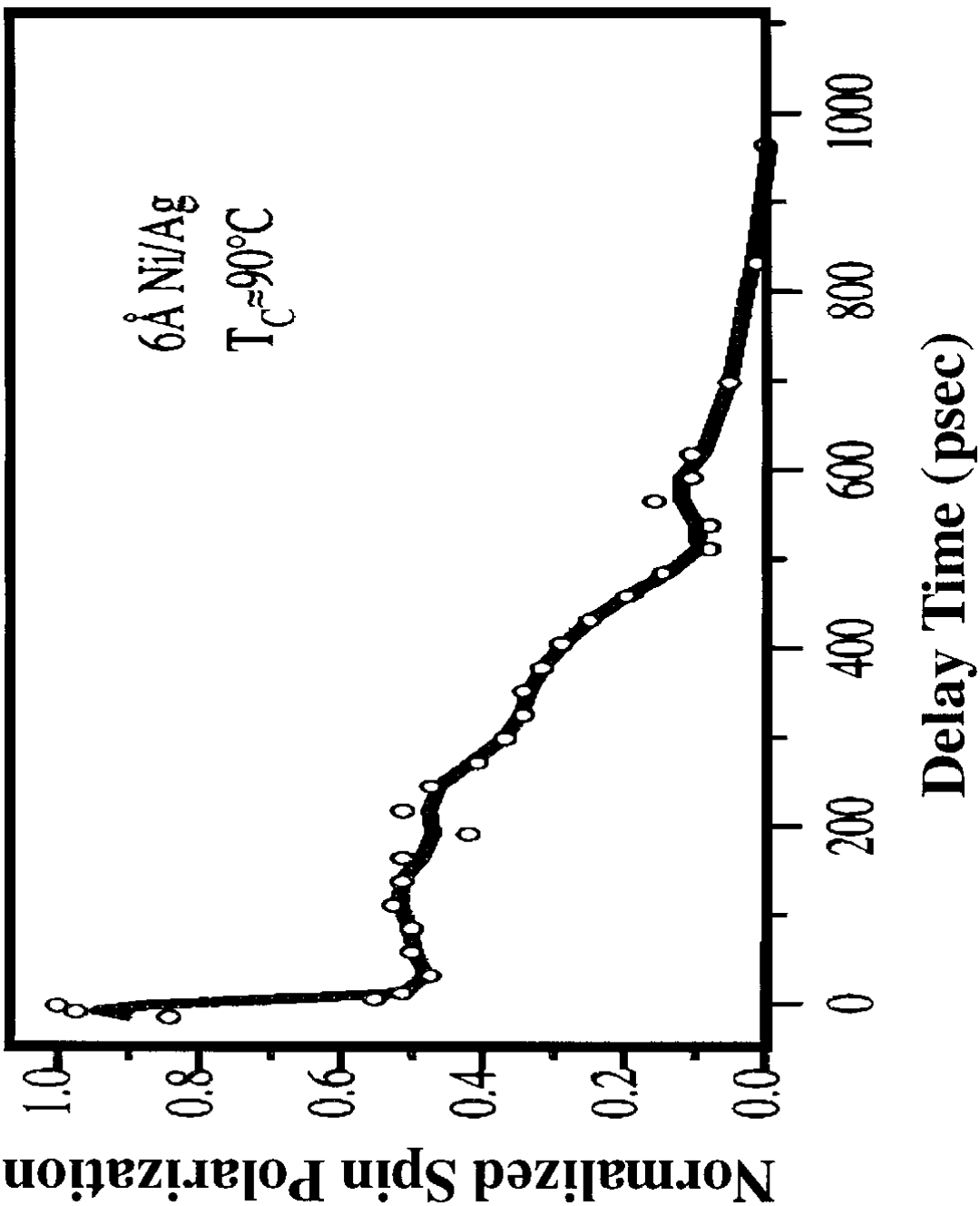
6Å Ni/Ag
T_C≈90°C
Normalized Spin Polarization
1.0
0.8
0.6
0.4
0.2
0.0
0
200
400
600
800
1000
Delay Time (psec)

Figure 6

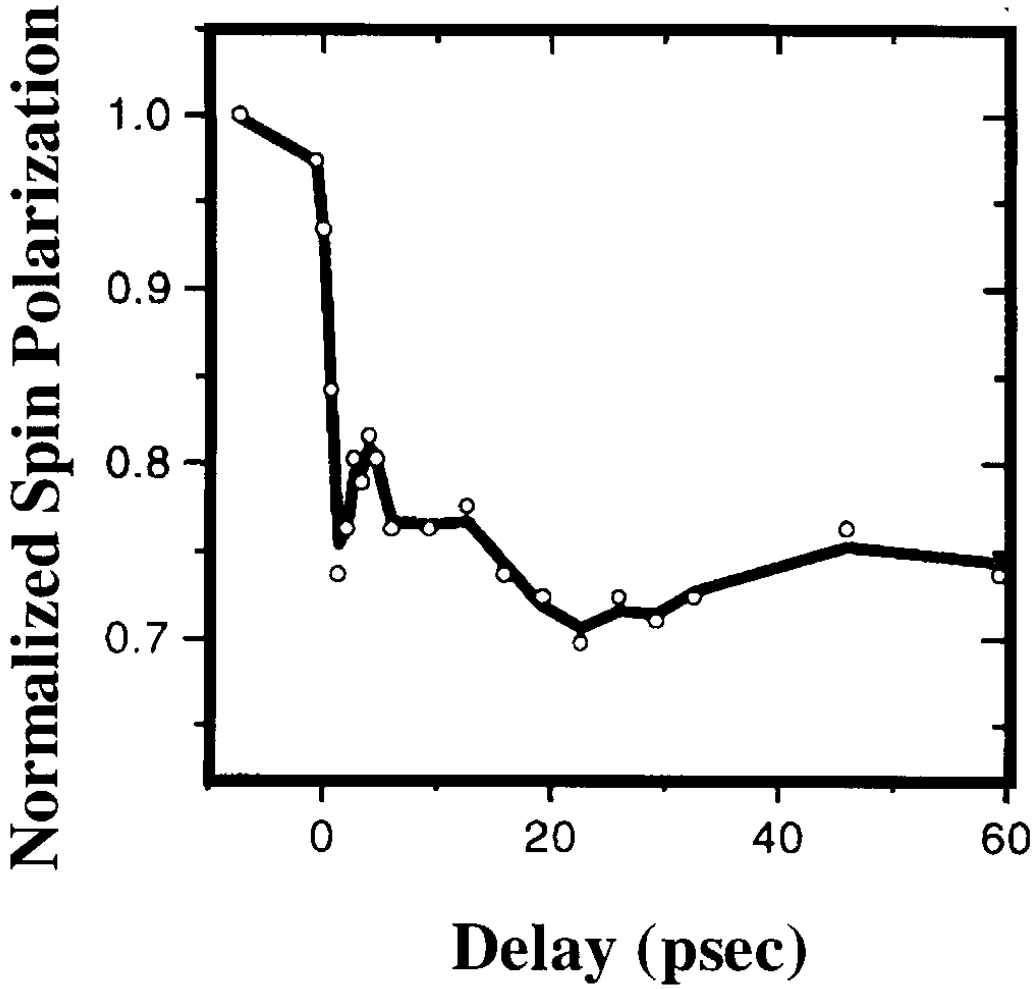
Normalized Spin Polarization
1.0
0.9
0.8
0.7
0
20
40
60
Delay (psec)

Figure 7